Available online at www.sciencedirect.com
SCIENCE DIRECT
Journal of Power Sources 154 (2006) 351–359
JOURNAL OF POWER SOURCES
www.elsevier.com/locate/jpowsour

Ethanol electro-oxidation on carbon-supported Pt, PtRu and Pt_3Sn catalysts: A quantitative DEMS study

H. Wang, Z. Jusys *, R.J. Behm

Department Surface Chemistry and Catalysis, University of Ulm, D-89069 Ulm, Germany

Available online 28 November 2005

Abstract

The electrocatalytic activity of commercial carbon supported PtRu/Vulcan and Pt_3Sn/Vulcan bimetallic catalysts (E-TEK, Inc.) for ethanol oxidation under well defined electrolyte transport conditions and their selectivity for complete oxidation were evaluated using cyclic voltammetry combined with on-line differential electrochemistry mass spectrometry (DEMS) measurements and compared to the activity/selectivity of standard Pt/Vulcan catalysts. The main reaction products CO_2, acetaldehyde and acetic acid were determined quantitatively, by appropriate calibration procedures, current efficiencies and product yields were calculated. Addition of Ru or Sn in binary Pt catalysts lowers the onset potential for ethanol electro-oxidation and leads to a subtle increase of the total activity of the Pt_3Sn/Vulcan catalyst. It does not improve, however, the selectivity for complete oxidation to CO_2, which is about 1% for all three catalysts under present reaction conditions—incomplete ethanol oxidation to acetaldehyde and acetic acid prevails on all three catalysts. The results demonstrate that the performance of the respective catalysts is limited by their ability for C–C bond breaking rather than by their activity for the oxidation of poisoning adsorbed intermediates such as CO_{ad} or $CH_{x,ad}$ species.

Keywords: Ethanol oxidation; Pt/Vulcan; PtRu/Vulcan; Pt_3Sn/Vulcan; DEMS; Product distribution

1. Introduction

Direct alcohol fuel cells (DAFCs) have attracted considerable interest in recent years because of their potential for portable applications. Since ethanol is the major renewable bio-fuel and less toxic than other alcohols, it is a promising alternative liquid fuel for directly fueled DAFC systems [1–3]. Complete oxidation of ethanol to CO_2, however, involves the cleavage of the C–C bond, which requires a rather high activation energy. In order to obtain reasonable rates at not too high overpotentials, novel membrane materials allowing operation at elevated temperatures and/or more active electrocatalysts are urgently needed. Strategies for the development of novel catalytic materials and the design of highly active catalysts for DAFC applications largely depend on a detailed understanding of the reaction mechanism and in particular of the rate-limiting step(s) during ethanol electro-oxidation under continuous reaction conditions. Despite significant efforts and numerous studies [4], however, the mechanism of the ethanol electro-oxidation reaction (EOR) still remains unclear or even contradictory. There is general agreement that ethanol electro-oxidation proceeds via a complex multi-step mechanism, which involves a number of adsorbed intermediates and also leads to different by-products for incomplete ethanol oxidation [5]. Adsorbed CO, C_1 and C_2 hydrocarbon residues have been identified as major adsorbed intermediates by means of in situ infrared spectroscopy [6,7] and differential electrochemical mass spectrometry (DEMS) [8,9], while acetaldehyde and acetic acid have been detected as the main by-products using infrared spectroscopy [7], on-line DEMS [1,2,6,10–14], ion chromatography and liquid chromatography [3,5].

Previous studies of the ethanol electro-oxidation reaction, applying both electrochemical and other physico-chemical probes, concentrated on solid Pt electrodes as the standard model catalyst in order to gain a fundamental understanding of the ongoing processes and the contributing elementary reaction steps. Leung et al. [7] quantitatively detected adsorbed CO and CO_2, acetaldehyde and acetic acid products formed in ethanolic solutions on solid Pt electrodes by FTIR spectroscopy. Applying chromatographic analysis Hitmi et al. [5] found for ethanol oxidation on polycrystalline Pt at 10 °C that at low ethanol concentrations (<0.01 M) acetic acid is the main product, whereas at high ethanol concentrations (>0.1 M) acetaldehyde formation prevails. Similar concentration effects on the EOR product yields

* Corresponding author. Tel.: +49 731 5025454; fax: +49 731 5025454.
E-mail address: zenonas.jusys@chemie.uni-ulm.de (Z. Jusys).

0378-7753/$ – see front matter © 2005 Elsevier B.V. All rights reserved.
doi:10.1016/j.jpowsour.2005.10.034

were reported for ethanol oxidation on carbon supported Pt electrocatalysts [15]. Tarnowski et al. [16] used ion chromatography to quantify the formation of acetic acid during room temperature constant potential ethanol oxidation on Pt(1 1 1), Pt(3 3 5) and Pt(5 5 7) electrodes and determined an increase in acetic acid formation with increasing step density. These results suggest that for ethanol electro-oxidation on solid Pt electrodes incomplete oxidation to acetaldehyde and acetic acid is the majority reaction pathway, rather than complete oxidation to CO_2. Incomplete ethanol oxidation, however, is highly undesirable for DAFC applications due to the inefficient use of the fuel and in particular because of toxic pollutant emissions.

A common way for improving the catalytic activity for ethanol electro-oxidation and the selectivity for complete oxidation is the use of bimetallic catalysts, which usually involves the addition of oxophilic metals such as Ru [1,2,17] or Sn [18,19]. Studying ethanol oxidation on Pt and PtRu electrodes electrodeposited on a Au substrate by DEMS, Fujiwara et al. could show that PtRu gives a higher relative yield of CO_2 than pure Pt, up to 100% for PtRu at low temperatures (5 and 25 °C) [2]. Wang et al. [1] studied the relative product distribution during polymer electrolyte fuel cell (PEFC) operation at temperatures between 150 and 190 °C with ethanol as the anode feed gas using on-line mass spectrometry. They found that acetaldehyde is the main product; while CO_2 is a minority product for ethanol concentrations (water/ethanol molar ratio) between 5 and 2, and that there is no differences in the product distribution over Pt-Ru and Pt-black. On the other hand, Arico et al. [17] reported a high selectivity towards CO_2 formation (95%) on a PtRu/Vulcan for ethanol electro-oxidation in a liquid-feed PEFC operating at 145 °C and 1 M ethanol. Vigier et al. [20] observed an enhanced overall activity for ethanol electro-oxidation over PtSn/Vulcan catalysts at low potentials using chromatographic techniques, in agreement with data previously reported [18,19]. Also in their case incomplete oxidation with acetaldehyde and acetic acid as main reaction products prevailed, accompanied by trace amounts of CO_2. In a very recent in situ IR study, Lamy et al. [21] resolved the formation of poisoning CO_{ad} species and their oxidation at potentials positive of 0.4 V during for ethanol oxidation on a PtSn/Vulcan catalyst. Finally, ethanol oxidation on Pt, PtRu and PtRh electrodes has also been studied using DEMS [1,2,6,10–14], but the absolute product yields and their distribution were not determined quantitatively.

So far, most of the previous studies dealt with ethanol electro-oxidation either on massive model catalysts (single crystal or polycrystalline electrodes) or on realistic, but poorly characterized fuel cell membrane electrode assemblies (MEAs). Quantitative information on product yields and reaction pathways for ethanol oxidation on realistic catalysts operating under well-defined fuel cell relevant conditions is lacking. Therefore, we started a detailed study of the mechanism and kinetics of the EOR over realistic, carbon supported catalysts under well-defined fuel cell relevant conditions (realistic catalysts, elevated temperatures, continuous mass transport), using on-line DEMS as a probe for qualitative and quantitative analysis of surface and bulk reaction products. In two preceding publications [9,15], we have addressed ethanol and acetaldehyde adsorption and their anodic (oxidative) and cathodic (reductive) desorption products on a Pt/Vulcan catalyst [9] as well as mechanistic details of ethanol bulk oxidation over Pt/Vulcan catalyst as a function of ethanol concentration, reaction temperature and catalyst loading [15]. In the present paper, we investigate ethanol electro-oxidation over commercial carbon-supported, bimetallic PtRu/Vulcan and Pt_3Sn/Vulcan alloy catalysts (E-TEK, Inc.)—the superior state-of-the-art compositions for the oxidation of poisoning, adsorbed CO species via a 'bifunctional' mechanism [22]—and compare their activity and selectivity for complete ethanol oxidation with those of a standard Pt/Vulcan catalyst. Based on on-line DEMS measurements in a dual thin-layer flow cell set-up, we determined the Faradaic current (charge) and the corresponding partial currents (charges) for CO_2, acetaldehyde and acetic acid formation under continuous mass transport conditions, and calculated the current efficiencies and relative product yields of CO_2, acetaldehyde and acetic acid during ethanol bulk oxidation on Pt/Vulcan, PtRu/Vulcan and Pt_3Sn/Vulcan catalysts. Finally, we conclude on possible implications of these results for the further optimization of anode catalysts for DAFCs.

2. Experimental

2.1. DEMS set-up and experimental details

The DEMS set-up consists of two differentially pumped chambers, a Balzers QMS 112 quadrupole mass spectrometer, a Pine Instruments potentiostat and a computerized data acquisition system. It is described in more detail in Ref. [23].

The thin film Pt/Vulcan, Pt_1Ru_1/Vulcan and Pt_3Sn/Vulcan (20 wt.% metal, E-TEK Inc.) electrodes for the DEMS measurements were prepared by pipetting and drying 20 μl aqueous catalyst suspension (2 mg/ml), and then, 20 μl aqueous Nafion solution in the center of mirror-polished glassy carbon disks (Sigradur G from Hochtemperatur Werkstoffe GmbH, 9 mm in diameter). The resulting catalyst thin film had a diameter of ca. 6 mm, a geometric surface area of 0.28 cm^2, and a metal loading of 28 μg cm^{-2} (for details see Ref. [24]).

The electrode was mounted into a dual thin-layer flow-through DEMS cell [23] and pressed against a ca. 50 μm thick spacer. This leaves an exposed area of 0.28 cm^2 and results in an electrolyte volume of ca. 5 μl at the working electrode. The electrolyte flow was driven by the hydrostatic pressure in the supply bottle (flow rate about 5–6 μl s^{-1}), ensuring a fast transport of the species formed at the electrode to the mass spectrometric compartment, where the volatile products were evaporated into the mass spectrometer (time constant ca. 2 s) through a bare porous membrane (Scimat, 60 μm thick, 50% porosity, 0.2 μm pore diameter).

Two Pt wires at the inlet and outlet of the thin-layer cell, connected through an external resistance (1 MΩ), were used as the counter electrodes. A saturated calomel electrode (SCE), connected to the outlet of the DEMS cell via a Teflon capillary, served as a reference electrode. All potentials, however, are quoted against that of the reversible hydrogen electrode (RHE).

The supporting electrolyte was prepared using Millipore Milli Q water and ultrapure sulfuric acid (Merck, suprapur). Ethanol (LiChrosolv) was obtained from Merck, CO (N4.7) from Messer-Griesheim. Before measurements, all solutions were deaerated by high-purity Ar (MIT Gase, N6.0). All experiments were carried out at room temperature (23 ± 1 °C).

2.2. Calibration of the DEMS set-up

To avoid interferences between the ion currents of the major ethanol electro-oxidation products CO_2^+ and CH_3CHO^+, which are both at $m/z = 44$, the formation of carbon dioxide and acetaldehyde were monitored individually at $m/z = 22$ (doubly ionized CO_2^{++}, 2.8% of the main $m/z = 44$ CO_2 peak) and $m/z = 29$ (COH^+ main fragment, 220% of the $m/z = 44$ acetaldehyde peak), respectively.

The average current efficiency for complete ethanol electro-oxidation to CO_2 per one carbon atom (12 electrons per ethanol molecule) was calculated using the following equation:

$$A_q(CO_2) = \frac{6Q_i}{(K^*_{22}Q_f)} \quad \text{or} \quad A_i(CO_2) = \frac{6I_i}{(K^*_{22}I_f)}, \tag{1}$$

where Q_f and I_f are the Faradaic charge and Faradaic current during ethanol oxidation, respectively, and Q_i and I_i are the corresponding mass spectrometric charge and current of $m/z = 22$; the factor 6 refers to the number of electrons needed for formation of one CO_2 molecule from ethanol, and K^*_{22} is the calibration constant for $m/z = 22$ determined from CO_{ad} oxidation or CO bulk oxidation on a Pt catalyst. For CO_{ad} oxidation and CO bulk oxidation, respectively, K^*_{22} was calculated by:

$$K^*_{22} = \frac{2Q_i}{Q_f} \quad \text{or} \quad K^*_{22} = \frac{2I_i}{I_f}, \tag{2}$$

where Q_f and I_f are the Faradaic charge and the Faradaic current during CO_{ad} oxidation and CO bulk oxidation, respectively, and Q_i and I_i are the corresponding mass spectrometric charge and current of $m/z = 22$. The factor 2 refers to the number of electrons needed for formation of one CO_2 molecule from CO_{ad} or bulk CO.

The current efficiency of acetaldehyde formation was calculated in the same way, using the following equation:

$$A_q(CH_3CHO) = \frac{2Q_i}{(K^*_{29}Q_f)} \quad \text{or} \quad A_i(CH_3CHO) = \frac{2I_i}{(K^*_{29}I_f)}, \tag{3}$$

where K^*_{29} was determined from measurements of the selective oxidation of ethanol to acetaldehyde on an electrodeposited Au film electrode at high potentials (>1.6 V) and high ethanol concentrations (>0.5 M). Here, we make use of the well-known current efficiency for acetaldehyde formation on a Au electrode under these conditions of about 90% [25]:

$$K^*_{29} = \frac{2I_i}{(I^*_f 0.9)}. \tag{4}$$

Acetic acid formation could not be directly detected due to its low vapor pressure (see also Fig. 2b). Therefore, acetic acid yields were determined indirectly, calculating the difference between the measured Faradaic current and the partial currents of ethanol oxidation to CO_2 and acetaldehyde, determined from the corresponding ion currents as described above. In this calculation, we assumed that only three ethanol oxidation products are formed, namely CO_2, acetaldehyde and acetic acid.

The individual product yields (W_i) were calculated from the corresponding current efficiencies ($A_{q,i}$) via $W_i = (A_{q,i}/n_i)/\sum_i A_{q,i}/n_i$, where n_i is the number of electrons required for ethanol oxidation reaction to the respective products (two electrons per molecule ethanol for acetaldehyde, four electrons for acetic acid, and six electrons for CO_2 formation, respectively). In addition, we have qualitatively monitored the formation of methane and ethane at low potentials (0.3–0.06 V) using the mass signals $m/z = 15$ (CH_3^+ fragment of methane) and $m/z = 30$ (molecular ion of ethane, $C_2H_6^+$).

3. Results and discussion

3.1. Ethanol oxidation on a Pt/Vulcan catalyst

A cyclic voltammogram (CV) and the corresponding mass spectrometric cyclic voltammograms (MSCVs) for ethanol oxidation on a Pt/Vulcan electrode in 0.1 M (solid lines) and 0.01 M (dotted lines) ethanol containing 0.5 M H_2SO_4 solution, which were recorded during repetitive cycling, are shown in Fig. 1. The

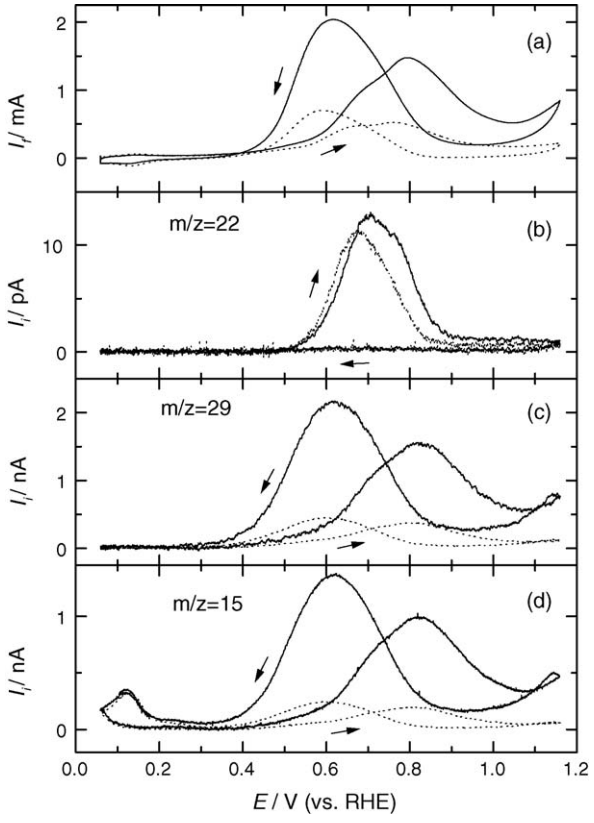

Fig. 1. Simultaneously recorded CVs (a) and MSCVs for $m/z = 22$ (b), $m/z = 29$ (c), $m/z = 15$ (d) for the oxidation of ethanol on a Pt/Vulcan catalyst in 0.1 M ethanol + 0.5 M H_2SO_4 (—) and in 0.01 M ethanol + 0.5 M H_2SO_4 (·····) solution (scan rate: 10 mV s^{-1}). Arrows indicate the direction of potential scan.

steady-state cyclic voltammogram for ethanol electro-oxidation on Pt/Vulcan catalyst (Fig. 1a) largely resembles those reported for polycrystalline Pt electrodes [6,13]. At potentials below ca. 0.4 V ethanol electro-oxidation is almost completely inhibited by adsorbed poisoning intermediates (CO and hydrocarbon residues [9]). It occurs at an appreciable rate only once these intermediates start to be oxidized at potentials positive of ca. 0.5 V, which results in an ill-resolved double peak in the positive-going scan. At higher potentials, the reaction is first hindered by PtO formation and then increases again at the positive potential limit. In the negative-going scan, ethanol oxidation sets in with PtO reduction negative of ca. 0.85 V, and decreases at more negative potentials due to re-poisoning of the catalyst. The interplay of these factors results in the hysteresis of the corresponding anodic current peak maxima for positive- and negative-going scans. The role of the ethanol concentration is reflected by the dotted line in Fig. 1a, which shows that a 10-fold decrease in ethanol concentration results only in ca. 4-fold decrease in Faradaic current (Fig. 1a).

The formation of CO_2, which was selectively followed by monitoring the doubly ionized molecular ion signal at $m/z = 22$ (see Section 2), starts at ca. 0.5 V in the positive-going scan (Fig. 1b), and then passes through an ill-resolved double peak with maxima ca. 0.7 and 0.77 V. At higher potentials, CO_2 formation continues at a steady small rate. The first peak for CO_2 production coincides with the first peak in the Faradaic current (Fig. 1a), but different from the Faradaic current signal it is the dominant one for CO_2 formation. Interestingly, the total amount of CO_2 formed during potentiodynamic ethanol bulk oxidation is comparable to that observed for ethanol adsorbate stripping [9] (taking into account the ratio of $m/z = 22$–44 ion signals for CO_2 (2.8%)), and also to that obtained for bulk ethanol oxidation at different concentrations. These observations suggest that CO_2 formation during the positive-going scan is mostly related to the oxidation of adsorbed CO species to CO_2. The slight broadening of the CO_2 formation peak compared to the stripping data is attributed to additional CO_{ad} formation due to C–C bond dissociation during ethanol electro-oxidation. The pronounced second peak in the Faradaic current for ethanol oxidation (positive-going scan, Fig. 1a) in combination with the low CO_2 formation rate at these potentials (Fig. 1b) suggests formation of other ethanol oxidation products in addition to CO_2. In the negative-going scan, CO_2 formation is inhibited over the entire potential range (Fig. 1b), although the Faradaic current exhibits a distinct peak centered at ca. 0.6 V (Fig. 1a). These findings agree well with DEMS data reported for ethanol oxidation on sputtered Pt electrodes [26].

The onset of acetaldehyde formation, which was selectively monitored via the CHO^+ fragment of acetaldehyde at $m/z = 29$ (see Section 2), occurs at potentials positive of ca. 0.35 V in the positive-going scan (Fig. 1c), simultaneously, with the onset of the ethanol oxidation current (Fig. 1a). In combination with the absence of CO_2 formation at potentials below 0.4 V (Fig. 1b) this suggests that at low potentials incomplete oxidation of ethanol is the dominant reaction pathway, in agreement with previous IR data [7]. Acetaldehyde formation increases with electro-oxidation of CO_{ad} species (CO_2 formation peak, Fig. 1b) during the positive-going scan, and results in a peak for acetaldehyde formation ($m/z = 29$) at ca. 0.8 V. This peak corresponds to the second anodic current peak. At even higher potentials, the CHO^+ signal follows the Faradaic current (Fig. 1a). Together with the low CO_2 formation rate at these potentials (Fig. 1b), this implies that incomplete ethanol oxidation prevails also at more positive potentials, positive of the main current peak. In the negative-going scan (Fig. 1c), acetaldehyde formation follows the Faradaic current (Fig. 1a). Taking into account the barely measurable CO_2 formation rate in the negative-going scan (Fig. 1b) this means that under these conditions ethanol oxidation is dominated by the incomplete oxidation pathway. The acetaldehyde formation rate decreases to about 1/6 upon decreasing the ethanol concentration from 0.1 (Fig. 1c, solid line) to 0.01 M (Fig. 1c, dotted line), i.e., the decay is more pronounced than in the Faradaic current signal.

The other major ionic fragment from acetaldehyde decomposition is CH_3^+, which results in the ion current at $m/z = 15$ (Fig. 1d). This signal exactly follows the features of the $m/z = 29$ ion current (Fig. 1c) at potentials positive of 0.3 V, indicating that both ions result from the same parent molecule (H_3C–CHO). However, in contrast to the featureless shape of the $m/z = 29$ signal at potentials below 0.3 V (Fig. 1c), the $m/z = 15$ ion current displays new features during the negative-going scan at these potentials (Fig. 1d). These are attributed to cathodic methane formation, in agreement with previous data obtained on a porous Pt electrode [6,10,12]. Similar methane formation characteristics were observed after (dissociative) ethanol adsorption at 0.66 V on a Pt/Vulcan catalyst in the subsequent negative-going scan (ethanol adsorbate stripping) in the H_{upd}-region [9], suggesting that also in ethanol-containing solution methane is formed by cathodic reduction of the adsorbed species at potentials <0.3 V, most likely of hydrocarbon residues, rather than by bulk reduction of ethanol to methane [12]. The formation of CH_4 is nearly independent of the concentration of ethanol (Fig. 1d), which also supports the above conclusion. Cathodic ethane production from ethanol is barely detectable on a Pt/Vulcan catalyst [21], and constitutes only 2–5% of the amount of methane formation (Fig. 1d), in contrast to the ca. 50% ethane reported in the literature for a sputtered porous Pt electrode [12]. We found, recently, that continuous reduction of acetaldehyde to ethane occurs at 0.06 V on a Pt/Vulcan catalyst [27]. Therefore, the low cathodic ethane yields from ethanol in our potentiodynamic experiments compared to previous data [12] are tentatively explained by the continuous removal of the volatile reaction intermediate/side product acetaldehyde under continuous flow-through conditions in our experiments, which is not possible in the stagnant electrolyte used in previous experiments.

Due to the low volatility of acetic acid in the low concentration of solution (less than 1 mM), no potential dependence for $m/z = 60$ could be detected. However, ethylacetate ester can be detected (through the $m/z = 61$ fragment [1]) in the negative-going scan at high (0.5 M) ethanol concentration (Fig. 2b). The presence of fragments at $m/z = 61$, 73 and 88 at ratios typical for the ethylacetate mass spectrum [28] confirms the formation of ethylacetate, which is formed by a follow-on chemical reaction of the electrochemically formed acetic acid with ethanol

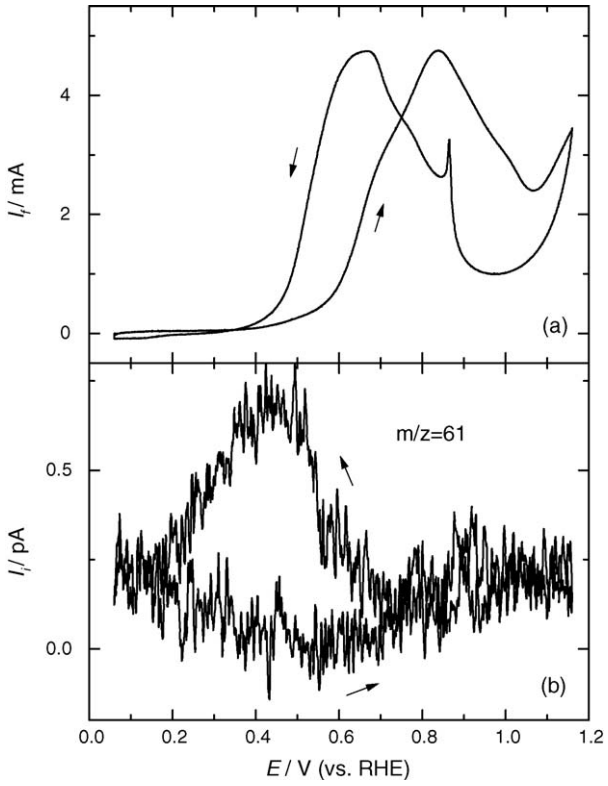

Fig. 2. Simultaneously recorded CVs (a) and MSCV for $m/z = 61$ (b) for the oxidation of ethanol on a Pt/Vulcan catalyst in 0.5 M ethanol + 0.5 M H_2SO_4 solution (scan rate: 10 mV s^{-1}). Arrows indicate the direction of potential scan.

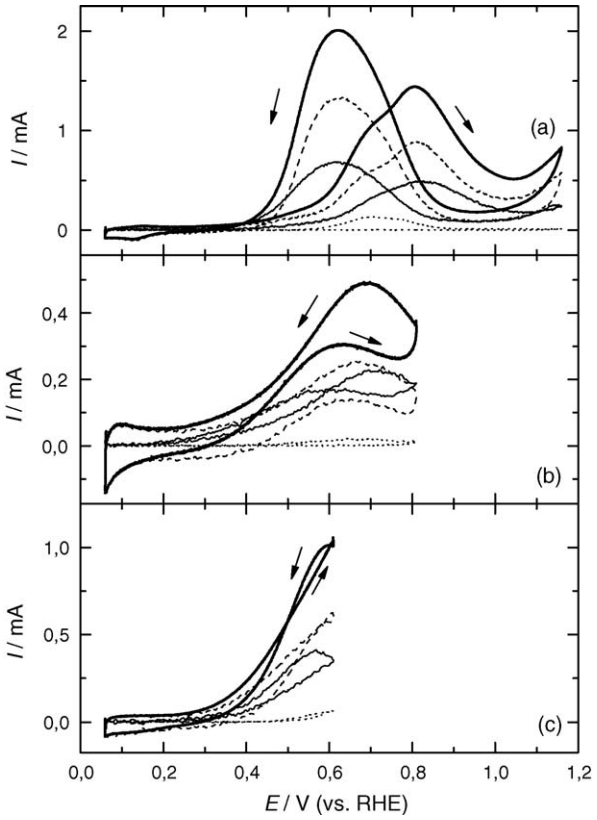

Fig. 3. Faradaic current signal and partial reaction currents during ethanol oxidation to CO_2 (dotted lines), acetaldehyde (thin solid lines) and acetic acid (dashed lines) over a: (a) Pt/C, (b) PtRu/C, and (c) Pt_3Sn/C catalyst electrode, as calculated from the data in Fig. 1 (Pt/Vulcan), 4 (PtRu/Vulcan) and 5 (Pt_3Sn/Vulcan). Arrows indicate the direction of potential scan.

according to:

$$CH_3COOH + CH_3CH_2OH \leftrightarrow CH_3COOCH_2CH_3 + H_2O. \quad (5)$$

The formation of ethylacetate occurs mainly in the negative-going scan. Its appearance, however, appears to be significantly delayed compared to the Faradaic current signal. Test experiments showed indeed that this delay is due to an experimental artifact, namely, slow ester permeation through the Teflon membrane due to the relatively large size of the molecule. Therefore, the acetic acid yields were determined indirectly, by calculating the difference between the measured Faradaic current and the partial currents for ethanol oxidation to CO_2 and acetaldehyde, which were determined from the corresponding ion currents as described in Section 2. The average current efficiencies for acetaldehyde, acetic acid, and CO_2 formation, integrated over a complete cycle in order to remove contributions from double-layer charging, were determined to ca. 37, 60, and 2.7% for 0.1 M ethanol solution, and 26, 68, and 6%, respectively, for 0.01 M ethanol solution. The corresponding product yields for acetaldehyde, acetic acid and CO_2 are 55, 44, 1% for 0.1 M ethanol solution, and 42, 55, 3% for 0.01 M ethanol solution (for a detailed discussion of the EOR product yields see [21]).

The partial reaction currents for ethanol oxidation to CO_2, acetaldehyde and acetic acid, which were calculated in the same way as described above, are depicted in Fig. 3a. These partial reaction current traces clearly demonstrate that the formation of acetaldehyde (thin solid line) and acetic acid (dashed line) largely follow the Faradaic current signal and by far dominate the latter signal. (Note that the acetic acid product current includes contributions from capacitive charging and metal oxidation.) The CO_2 related current is responsible for the slight shoulder cathodic of the main maximum in the positive-going scan. On an absolute scale, CO_2 formation is a minority pathway at all potentials, and the Faradaic current is dominated by the currents for the incomplete oxidation pathways.

3.2. Ethanol oxidation on a PtRu/Vulcan catalyst

In Fig. 4, we show similar steady-state CVs and MSCVs for ethanol electro-oxidation on a PtRu/Vulcan catalyst. The positive potential limit for the bimetallic catalysts was lower than for Pt/Vulcan to avoid leaching of the less-noble component. The PtRu/Vulcan catalyst shows a slight increase in the Faradaic current during the positive-going scan at low (0.2–0.4 V) potentials compared to the Pt/Vulcan catalyst, while at potentials positive of 0.5 V the ethanol oxidation current on PtRu/Vulcan is significantly lower than that on Pt/Vulcan (Fig. 1a). The onset of CO_2 formation on the PtRu/Vulcan catalyst in the positive-going scan occurs at ca. 0.4 V, compared to ca. 0.5 V on Pt/Vulcan. At potentials positive of 0.55 V, however, CO_2 formation on PtRu/Vulcan is much lower than for Pt/Vulcan. In the negative-going scan,

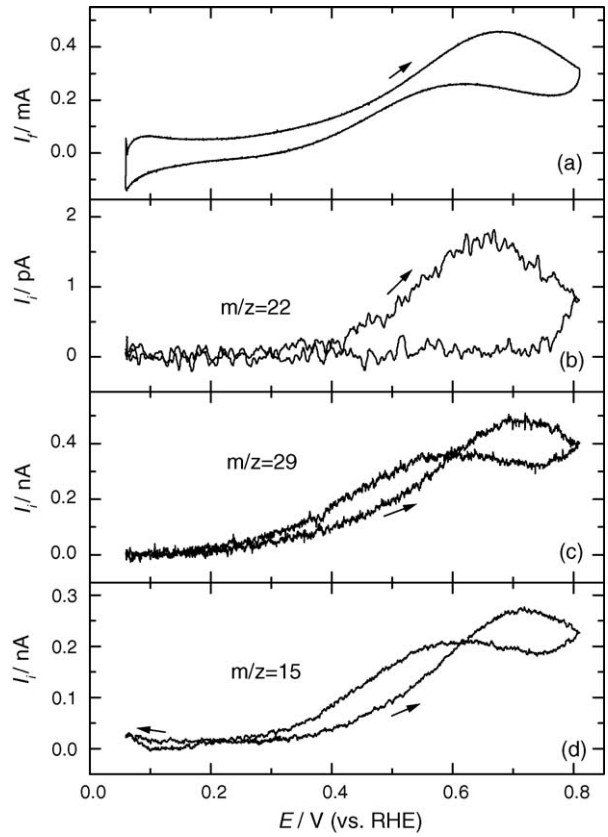

Fig. 4. Simultaneously recorded CVs (a) and MSCVs for $m/z = 22$ (b), $m/z = 29$ (c) and $m/z = 15$ (d) for the oxidation of ethanol on a PtRu/Vulcan catalyst in 0.1 M ethanol + 0.5 M H_2SO_4 solution (scan rate: 10 mV s^{-1}). Arrows indicate the direction of potential scan.

CO_2 formation is inhibited on the PtRu/Vulcan catalyst (Fig. 4b), similar to our findings for the Pt/Vulcan catalysts. Hence, we can conclude already from these qualitative results that also, in this case, incomplete ethanol oxidation prevails in the negative-going scan. Acetaldehyde formation, monitored via its fragment at $m/z = 29$, starts at ca. 0.2 V on the PtRu/Vulcan catalyst during the positive-going scan and is higher than on the Pt/Vulcan catalyst up to ca. 0.6 V, whereas at more positive potentials, the rate for acetaldehyde formation is higher on the Pt/Vulcan catalyst (Fig. 1c). In contrast to the inhibited CO_2 formation, acetaldehyde production occurs also in the negative-going scan on the PtRu/Vulcan catalyst (Fig. 4c).

As discussed above, the $m/z = 15$ ion current (Fig. 4d) originates from the acetaldehyde fragment at potentials positive of 0.3 V, and therefore, follows the $m/z = 29$ signal (Fig. 4c). Interestingly, the cathodic desorption of methane, which occurs at potentials negative of 0.3 V on the Pt/Vulcan catalyst (Fig. 1d), is barely detectable on the PtRu/Vulcan catalyst (Fig. 4d), and ethane formation is completely absent (not shown). This result contrasts previous reports on ethanol oxidation on porous PtRu catalysts containing 8 or 15 at.% Ru, where methane and ethane were detected as cathodic desorption products in ethanol containing solution, with decreasing amounts of methane and ethane formed with increasing Ru content [12]. The discrepancy between the literature data [12] and our DEMS results may be explained by different effects, (i) by the much higher Ru content in the present catalysts compared to the 8 and 15% in the electrodes in Ref. [12], (ii) by the different morphology and porosity of the thin-film electrode compared to the electrodeposited porous PtRu layers in Ref. [12], and (iii) by the enforced convection in the present study, as compared to stagnant electrolyte in Ref. [12]. The data in Ref. [12] showed already a marked decline in ethane formation when going from 8 to 15%, and a further increase in Ru content to 50% may be sufficient to completely inhibit this pathway. The other two effects both affect the removal of incomplete oxidation products such as acetaldehyde, from the PtRu catalyst, which may be accumulated in the vicinity of the electrode or entrapped in the porous catalyst layer in the absence of enforced convection. In that case, subsequent cathodic reduction of acetaldehyde to ethane would be possible [9,27]. These effects are largely suppressed under the continuous flow conditions characteristic for our experiments.

Our DEMS results suggest that at low potentials (0.2–0.4 V) ethanol oxidation on PtRu/Vulcan catalyst results exclusively in incomplete oxidation products, although it is difficult to quantify the corresponding yields for acetaldehyde and acetic acid at these low potentials in potentiodynamic measurements due to relatively large capacitive contributions at a low ethanol oxidation rate (low Faradaic current). A quantitative evaluation of the different partial reaction currents for ethanol oxidation to CO_2, acetaldehyde and acetic acid, which were calculated in the same way as described above, illustrates that incomplete ethanol oxidation dominates the Faradaic current signal at all potentials, and that under current reaction conditions, the contributions from acetaldehyde formation and acetic acid formation are of comparable magnitude and also comparable in shape (Fig. 3b). (Again the acetic acid product current includes contributions from capacitive charging and metal oxidation.) The average current efficiencies for CO_2, acetaldehyde and acetic acid formation for ethanol oxidation on PtRu/Vulcan catalyst in 0.1 M solution integrated over a complete potential cycle are ca. 2.6, 53 and 44%, compared to 2.7, 37 and 60% on Pt/Vulcan, respectively (see Table 1). The corresponding product yields for ethanol oxidation to CO_2, acetaldehyde and acetic acid on the PtRu/Vulcan catalyst are 1, 69 and 30%, compared to 1.4, 55 and 44% on the Pt/Vulcan, respectively (Table 1). Hence, the addition of Ru to Pt at a ratio of 1:1 has nearly no effect on the selectivity for CO_2 formation, while the selectivity for ethanol oxidation to acetaldehyde increases on the PtRu/Vulcan cata-

Table 1
Average current efficiencies (A_q) and product yields (W_q) for CO_2, CH_3CHO and CH_3COOH during ethanol oxidation over Pt/Vulcan, PtRu/Vulcan and Pt_3Sn/Vulcan catalysts, respectively, in 0.5 M H_2SO_4 + 0.1 M ethanol solution integrated over a complete potential cycle (confidence interval ca. 90%)

	Pt/Vulcan	PtRu/Vulcan	Pt_3Sn/Vulcan
$A_q(CO_2)$ (%)	2.7	2.6	2.6
$W_q(CO_2)$ (%)	1.3	1	1.2
$A_q(CH_3CHO)$ (%)	37	53	41
$W_q(CH_3CHO)$ (%)	55	69	59
$A_q(CH_3COOH)$ (%)	60	44	56
$W_q(CH_3COOH)$ (%)	44	30	40

lyst compared to Pt/Vulcan, and the selectivity for oxidation to acetic acid decreases correspondingly. These results apparently contradict the findings of Fujiwara et al. [2] and Arico et al. [17], who reported a high (up to 95%) selectivity for ethanol complete oxidation to CO_2 on a PtRu catalyst, which were performed at room temperature in a stagnant electrolyte [2] and in a liquid-feed DAFC operating at 145 °C [16], respectively. In the first case, this might be related to the low sensitivity of the experimental setup as well as re-adsorption and subsequent oxidation of the acetaldehyde intermediate in the stagnant electrolyte [2]. In the second study, we expect that the high reaction temperature leads to a significant increase of the rate for C–C bond breaking, which favors complete ethanol oxidation.

In general, however, the lower ethanol oxidation activity of the PtRu/Vulcan catalyst used in the present study compared to Pt/Vulcan agrees well with the results reported by Fujiwara et al. [2], where the activity of PtRu alloy catalyst for ethanol electro-oxidation was found to decrease with the increase in Ru content at Ru concentrations >10 at.%. Assuming: (i) that ethanol adsorption and C–C bond dissociation requires Pt ensembles to accommodate the resulting dissociative adsorption fragments (geometric ensemble effect [29]) and (ii) that Ru sites are inactive for ethanol adsorption/dissociation [2,12], the low activity of the Ru-rich catalyst for ethanol oxidation is easily explained by the limited number of such Pt ensembles in a catalyst with a homogeneous distribution of surface atoms, as it had been found for PtRu model catalysts [30]. This interpretation is supported by the low amount of methane desorbed cathodically (Fig. 4d) from the PtRu/Vulcan catalyst compared to Pt/Vulcan. Likewise, previous studies reported an optimum composition of PtRu catalysts for ethanol oxidation of between 8 and 33 at.% Ru [2,12], which considering that pure Ru is inactive for ethanol oxidation [2,12], also points to an ensemble effect, with larger Pt ensembles being required for C–C bond breaking, while on smaller Pt ensembles incomplete ethanol oxidation to acetaldehyde and acetic acid is favored. Hence, although Ru is an oxygen (OH_{ad}) supplier for the oxidation of adsorbed CO intermediates, via a bifunctional mechanism [22], higher Ru concentrations are not beneficial for ethanol oxidation due to the inhibition of C–C bond breaking caused by the lack of Pt ensembles. On the other hand, the relative amount of CO_2 formation during ethanol oxidation is comparable for the PtRu/Vulcan and for the Pt/Vulcan catalyst (see Table 1), which contrasts expectations based on a simple ensemble effect. Assuming that methane formation is generally less than CO_2 formation due to partial oxidation of $CH_{x,ad}$ species resulting from C–C bond breaking [8,13], this holds true also for the relative amount of C_1 (methane plus CO_2) formation in total, relative to C_2 (acetaldehyde plus acetic acid) formation.

3.3. Ethanol electro-oxidation on a Pt_3Sn/Vulcan catalyst

A cyclic voltammogram (CV) and the corresponding mass spectrometric cyclic voltammograms (MSCVs) for ethanol oxidation on Pt_3Sn/Vulcan catalyst, equally recorded during repetitive cycling, are shown in Fig. 5. In this case, the positive limit was lowered to 0.6 V to avoid Sn leaching. The addition of Sn

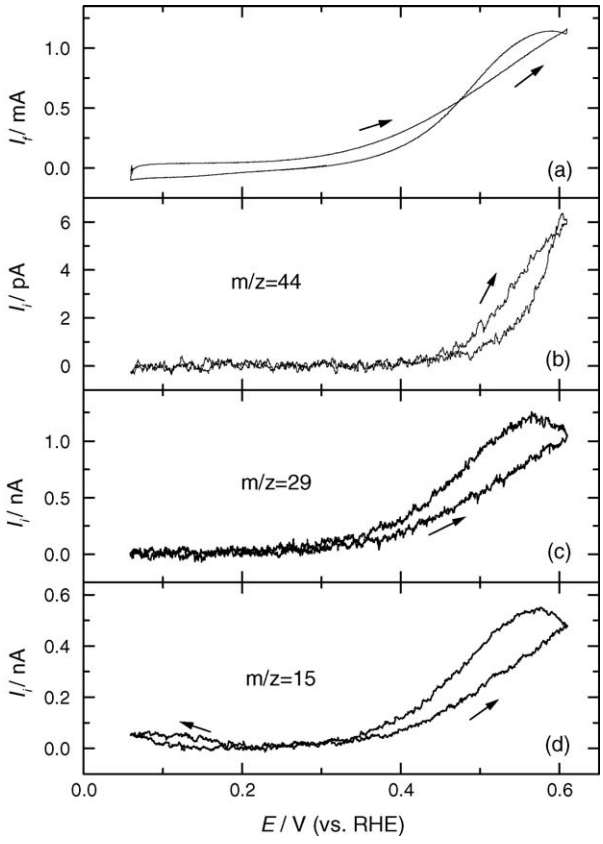

Fig. 5. Simultaneously recorded CVs (a) and MSCVs for $m/z = 22$ (b), $m/z = 29$ (c) and $m/z = 15$ (d) for the oxidation of ethanol on a Pt_3Sn/Vulcan catalyst in 0.1 M ethanol + 0.5 M H_2SO_4 solution (scan rate: 10 mV s^{-1}). Arrows indicate the direction of potential scan.

significantly enhances the oxidation of ethanol at low potentials (0.3–0.6 V) (Fig. 5a), compared to the Pt/Vulcan catalyst (Fig. 1a), in agreement with data reported previously [19,20,31]. The onset potential for CO_2 formation on Pt_3Sn/Vulcan catalyst in the positive-going scan is shifted negatively by ca. 0.1 V relative to the Pt/Vulcan catalyst, from 0.5 to 0.4 V (Fig. 1b). The onset of the anodic current for ethanol oxidation on Pt_3Sn/Vulcan catalyst, is at much lower potentials, at ca. 0.2 V (Fig. 5a), indicating incomplete ethanol oxidation (to acetaldehyde and acetic acid) at potentials negative of 0.4 V as dominant reaction path. Indeed, the onset of acetaldehyde formation occurs at ca. 0.2 V (Fig. 5c) and roughly follows the current–voltage dependence in Fig. 5a. The positive limit of 0.6 V is too low to ensure complete oxidation of the adsorbed CO and CH_x species, and therefore, CO_2 formation continues also in the negative going scan, down to a lower limit of about 0.4 V, where further reaction is limited by the lack of OH_{ad}. We expect that also at that point the adsorbed CO and CH_x species are not completely removed, which reduces the amount of subsequent ethanol adsorption in the lower potential region.

A quantitative evaluation of the different partial reaction currents for ethanol oxidation to CO_2, acetaldehyde and acetic acid, which is shown in Fig. 3c, leads to similar conclusions as on the other two catalysts. Incomplete ethanol oxidation dominates the Faradaic current signal at all potentials, and under current reac-

tion conditions the contributions from acetaldehyde formation and acetic acid formation are of comparable magnitude and also comparable in shape. The average current efficiencies and product distribution for CO_2, acetaldehyde and acetic acid formation, calculated for ethanol electro-oxidation on Pt_3Sn/Vulcan catalyst within one complete cycle as discussed above, are ca. 2.6, 41 and 56.4, and 1.2, 59 and 40%, respectively. These values are comparable to those for the Pt/Vulcan catalyst at the same (0.1 M) ethanol concentration (see Table 1). Hence, although ethanol oxidation is enhanced on the Pt_3Sn/Vulcan catalyst compared to Pt/Vulcan, the selectivity towards complete oxidation to CO_2 is similar for both catalysts, and CO_2 formation results most likely from the electro-oxidation of CO_{ad} species generated at lower potentials during the potential cycle. The latter conclusion is supported by recent IR spectroscopy studies on a Pt_4Sn/Vulcan catalyst [21], which show a decrease of linearly bonded CO_{ad} band intensity at potentials positive of 0.4 V, in agreement with our DEMS results (Fig. 5b). Moreover, our DEMS results are fully consistent with a high pressure liquid chromatography analysis of the long-term ethanol electrolysis products on a Pt_4Sn/Vulcan catalyst, which show only trace amounts of CO_2 over the entire potential up to 0.7 V, an enhanced activity for CO_{ad} oxidation at low potentials (>0.4 V) compared to that of a Pt/Vulcan catalyst, and a ratio of 0.6–0.7 for acetic acid formation to acetaldehyde formation at potentials between 0.4 and 0.7 V [20].

The amount of methane formed via cathodic desorption of hydrocarbon residues in the hydrogen region is strongly reduced on the Pt_3Sn/Vulcan catalyst (Fig. 5c) compared to Pt/Vulcan (Fig. 1c), to about 1/8 of the amount on Pt/Vulcan, and ethane formation is completely absent (not shown). The observation of CO_2 formation at potentials' positive of 0.4 V, which results most likely from CO_{ad} oxidation as discussed above, provides clear proof of dissociative ethanol adsorption, including C–C bond breaking, on the Pt_3Sn/Vulcan catalyst. This conclusion is supported also by IR data [21].

Ethanol C–C bond breaking upon adsorption should lead also to the formation of hydrocarbon residues co-adsorbed with CO_{ad} [9]. Assuming that Sn is inactive for ethanol adsorption/dissociation, the strongly reduced amount of cathodic methane formation on the Pt_3Sn/Vulcan catalyst can be explained in a similar way as for PtRu/Vulcan (see Section 3.2), via an ensemble effect. Also in this case, however, the relative amount of both C_1 product species together is comparable to that on the other two catalysts, showing that also in this case a simple ensemble model is not sufficient to explain the experimental observations.

Interestingly, the oxidation of CO_{ad} derived from ethanol adsorption on carbon supported Pt_3Sn catalysts starts later, at potentials positive of 0.4 V as found from DEMS (Fig. 5b) and IR measurements [21], than oxidation of a pre-adsorbed saturated CO_{ad} layer. In the latter case, CO_{ad} oxidation starts already at about 0.25 V, as had been shown for Pt_3Sn/Vulcan and Sn-modified Pt/Vulcan catalysts [32–34], $Pt_3Sn(1\,1\,1)$ [35,36], Sn-modified Pt(1 1 1) [37–39], and Sn-upd modified polycrystalline Pt [40]. Apparently, adsorption of ethanol on the Pt_3Sn/Vulcan catalyst does not populate the "weakly adsorbed" CO state, which is present for a saturated CO_{ad} layer created by CO adsorption from gaseous CO on PtSn alloys, and whose oxidation results in a low potential pre-peak [41].

4. Conclusions

We have demonstrated by combined cyclovoltammetric and on-line DEMS measurements under continuous flow conditions that at ambient temperatures and on realistic, carbon supported Pt, PtRu and Pt_3Sn fuel cell catalysts ethanol oxidation results predominantly in the incomplete oxidation products, acetaldehyde and acetic acid. Complete oxidation to CO_2 is a minority pathway at all potentials, contributing by about 1% to the total product yield under our conditions. For Pt/Vulcan, the total amount of CO_2 formation is little affected by the ethanol concentration, implying that it mainly results from oxidative removal of adsorbed CO and $CH_{x,ad}$ species generated from dissociative ethanol adsorption in the low potential region. In the hydrogen adsorption region, methane is formed as a reduction product of adsorbed hydrocarbon residues, generated by dissociative ethanol adsorption, with much lower methane yields on the binary catalysts than on Pt/Vulcan.

Addition of Ru or Sn in binary Pt catalysts lowers the onset potential for ethanol electro-oxidation and the onset for CO_{ad} oxidation. It does not, however, increase the selectivity for complete oxidation to CO_2—incomplete ethanol oxidation prevails also on these binary catalysts. While for Pt/Vulcan and Pt_3Sn/Vulcan the ratio of acetaldehyde to acetic acid formation is about equal, it is significantly higher for the PtRu/Vulcan catalyst.

The data demonstrate that the activity for ethanol oxidation not only depends on the ability of the respective catalyst for oxidative removal of poisoning CO_{ad} species, but also and in particular on its activity for C–C and C–H bond breaking. Therefore, the PtRu and Pt_3Sn catalysts, which are highly active for CO_{ad} oxidation, show only small improvements in the overall activity (Pt_3Sn), the selectivity for complete oxidation to CO_2 remains constant. Finally, these as well as literature data underline the need to not only improve the efficiency of fuel utilization in the DAFC, but also to avoid undesirable emissions of toxic emissions by increasing the selectivity of ethanol oxidation for complete oxidation.

Acknowledgements

We gratefully acknowledge financial support by the Deutsche Forschungsgemeinschaft (DFG) via grant Be 1201/12-1, and by the Landesstiftung Baden-Württemberg via the program 'Portable Mini Fuel Cells'.

References

[1] J. Wang, S. Wasmus, R.F. Savinell, J. Electrochem. Soc. 142 (1995) 4218.
[2] N. Fujiwara, K.A. Friedrich, U. Stimming, J. Electroanal. Chem. 472 (1999) 120.
[3] C. Lamy, E.M. Belgsir, J.M. Leger, J. Appl. Electrochem. 31 (2001) 799.

[4] S.G. Sun, in: J. Lipkowski, P.N. Ross (Eds.), Electrocatalysis, Wiley/VCH, New York, 1998, p. 243.
[5] H. Hitmi, E.M. Belgsir, J.M. Leger, C. Lamy, R.O. Lezna, Electrochim. Acta 39 (1994) 407.
[6] T. Iwasita, E. Pastor, Electrochim. Acta 39 (1994) 531.
[7] L.W.H. Leung, S.C. Chang, M.J. Weaver, J. Electroanal. Chem. 266 (1989) 317.
[8] U. Schmiemann, U. Mueller, H. Baltruschat, Electrochim. Acta 40 (1994) 99.
[9] H. Wang, Z. Jusys, R.J. Behm, Fuel Cells 4 (2004) 113.
[10] B. Bittins-Cattaneo, S. Wilhelm, E. Cattaneo, H.W. Buschmann, W. Vielstich, Ber. Bunsenges. Phys. Chem. 92 (1988) 1210.
[11] J.P.I. deSouza, S.L. Queiroz, K. Bergamaski, E.R. Gonzalez, F.C. Nart, J. Phys. Chem. 106 (2002) 9825.
[12] V.M. Schmidt, R. Ianniello, E. Pastor, S. Gonzalez, J. Phys. Chem. 100 (1996) 17901.
[13] J. Willsau, J. Heitbaum, J. Electroanal. Chem. 194 (1985) 27.
[14] R. Ianniello, V.M. Schmidt, J.L. Rodriguez, E. Pastor, J. Electroanal. Chem. 471 (1999) 167.
[15] H. Wang, Z. Jusys, R.J. Behm, J. Phys. Chem. B 108 (2004) 19413.
[16] D.J. Tarnowski, C. Korzeniewski, J. Phys. Chem. 101 (1997) 253.
[17] A.S. Arico, P. Creti, P.L. Antonucci, V. Antonucci, Electrochem. Solid-State Lett. 1 (1998) 66.
[18] C.T. Hable, M.S. Wrighton, Langmuir 9 (1993) 3284.
[19] F. Delime, J.-M. Leger, C. Lamy, J. Appl. Electrochem. 29 (1999) 1249.
[20] F. Vigier, C. Coutanceau, A. Perrard, E.M. Belgsir, C. Lamy, J. Appl. Electrochem. 34 (2004) 439.
[21] C. Lamy, S. Rousseau, E.M. Belgsir, C. Coutanceau, J.-M. Leger, Electrochim. Acta 49 (2004) 3901.
[22] M. Watanabe, S. Motoo, J. Electroanal. Chem. 60 (1975) 267.
[23] Z. Jusys, H. Massong, H. Baltruschat, J. Electrochem. Soc. 146 (1999) 1093.
[24] T.J. Schmidt, H.A. Gasteiger, G.D. Stäb, P.M. Urban, D.M. Kolb, R.J. Behm, J. Electrochem. Soc. 145 (1998) 2354.
[25] G. Tremiliosi-Filho, E.R. Gonzalenz, A.J. Motheo, E.M. Belgsir, J.-M. Leger, C. Lamy, J. Electroanal. Chem. 444 (1998) 31.
[26] T. Iwasita, J. Braz. Chem. Soc. 13 (2002) 401.
[27] H. Wang, Z. Jusys, R.J. Behm, J. Appl. Electrochem., in press.
[28] E. Stenhagen, S. Abrahamsson, F.W. McLafferty (Eds.), Atlas of Mass Spectral Data, Interscience, New York, 1969.
[29] W.M.H. Sachtler, Le Vide, 164 (1973) 67.
[30] H.E. Hoster, T. Hager, R.J. Behm, in preparation.
[31] C.T. Hable, M.S. Wrighton, Langmuir 7 (1991) 1305.
[32] J. Kaiser, Z. Jusys, R.J. Behm, R. Mörtel, H. Bönnemann, in: F.N. Buchi, G. Scherer, A. Wokaun (Eds.), Proceedings of the First European PEFC Forum, Lucerne, Switzerland, 2001, p. 59.
[33] A. Manzo-Robledo, A.-C. Boucher, E. Pastor, N. Alonso-Vante, Fuel Cells 2 (2002) 109.
[34] E.M. Crabb, R. Marshall, D. Thompsett, J. Electrochem. Soc. 146 (2000) 4440.
[35] K. Wang, H.A. Gasteiger, N.M. Markovic, P.N. Ross Jr., Electrochim. Acta 41 (1996) 2587.
[36] V.R. Stamenkovic, M. Arenz, C.A. Lucas, M.E. Gallagher, P.N. Ross, N.M. Markovic, J. Am. Chem. Soc. 125 (2003) 2736.
[37] H. Massong, H. Wang, G. Samjeske, H. Baltruschat, Electrochim. Acta 46 (2000) 701.
[38] B.E. Hayden, M.E. Rendal, O. South, J. Am. Chem. Soc. 125 (2003) 7738.
[39] S. Tillmann, G. Samjeske, K.A. Friedrich, H. Baltruschat, Electrochim. Acta 49 (2003) 73.
[40] Y. Morimoto, E.B. Yeager, J. Electroanal. Chem. 444 (1998) 95.
[41] H.A. Gasteiger, N.M. Markovic, P.N. Ross, J. Phys. Chem. 99 (1995) 8945.